CASE 2: EXPERIMENTAL EVALUATION OF AN ISOLATED SYNTHETIC JET IN CROSSFLOW

Norman W. Schaeffler, Luther N. Jenkins, and Timothy E. Hepner

Flow Physics & Control Branch, NASA Langley Research Center, Hampton, VA 23681-2199

Introduction

The second case for this workshop builds upon the isolated synthetic jet of Case 1 by adding a crossflow, with no streamwise pressure gradient, for the developing jet to interact with. Formally, Case 2 examines the interaction of a single, isolated, synthetic jet and a fully turbulent zero-pressure gradient boundary layer. The resulting flow has many of the characteristics that need to be modeled with fidelity if the results of the calculations are to serve as the basis for research and design with active flow control devices. These include the turbulence in the boundary layer, the time-evolution of the large vortical structure emanating from the jet orifice and its subsequent interaction with and distortion by the boundary layer turbulence, and the effect of the suction cycle on the boundary layer flow.

In a synthetic jet, the flow through the orifice and out into the outer flowfield alternates between an exhaust and a suction cycle, driven by the contraction and expansion of a cavity internal to the actuator. In the present experiment, the volume changes in the internal cavity are accomplished by replacing one of the rigid walls of the cavity, the wall opposite the orifice exit, with a deformable wall. This flexible wall is driven by a bottom-mounted moveable piston. The piston is driven electro-mechanically. The synthetic jet issues into the external flow through a circular orifice. In the present experiment, this orifice has a diameter of 0.250 inches (6.35 mm). The flow is conceptually similar to that documented in Schaeffler [1].

To document the flow, several measurement techniques were utilized. The upstream boundary conditions (in-flow conditions), and several key phase-averaged velocity profiles were measured with a 3-component laser-Doppler velocimetry system. Phase-averaged velocity field measurements were made with both stereo digital particle image velocimetry and 2-D digital particle image velocimetry as the primary measurement system. Surface pressure measurements were made utilizing an electronically scanned pressure system.

Facility and Actuator Details

This research effort was conducted in the NASA Langley 15-inch Low Speed Wind Tunnel of the Flow Physics and Control Branch. This tunnel is a closed-return atmospheric facility dedicated to basic flow physics research efforts. The tunnel has a maximum speed of 115 ft/s and a turbulence intensity of less than 0.13%. The tunnel medium is air at sea level conditions. During this research effort, the tunnel was equipped with a suspended flat plate model that acts a splitter plate and facilitates the installation of the actuator within the plate model. The plate features an elliptical leading edge. Immediately downstream of the transition from the leading edge to the plate, there is a grit strip to trip the boundary layer of the plate and also grit strips at corresponding locations on the tunnel walls. The ceiling of this tunnel is adjustable at several locations down the length of the tunnel. The ceiling height was adjusted to create a zero pressure gradient over the plate starting from a station 24.8 inches (630 mm) downstream from the leading edge to a station 58.8 inches (1494 mm) downstream from the leading edge. The centerline of the jet was located 38.8 inches (986 mm) downstream of the leading edge. This results in the region of zero pressure gradient

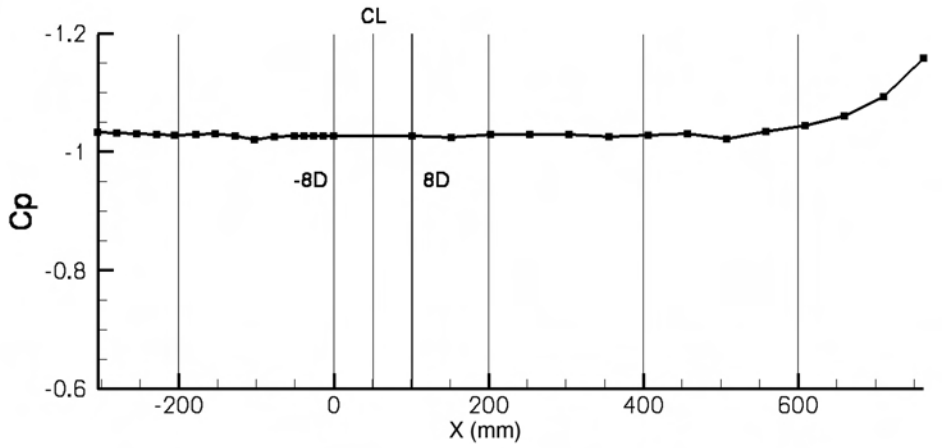

Figure 1: Pressure distribution down the centerline of the tunnel. X is measured in the streamwise direction, and X = 0.00 is the origin of the model coordinate system. The model coordinate system is shown schematically in Figure 4.

extending 56 jet diameters upstream of the jet centerline and 80 jet diameters downstream, as shown in Figure 1. These pressures were measured via a row of static pressure taps which are installed along the centerline of the tunnel with a total of 15 taps upstream of the jet exit and 15 taps downstream of the jet centerline, or exit. A set of spanwise pressure taps, 16 in total, were located 8 jet diameters upstream of the jet centerline and another set of spanwise taps, also 16 in total, were located 8 jet diameters downstream. All of these taps were connected via short lengths of flexible Tygon tubing to two ESP scanning pressure transducers, each with a full scale range of $\pm$10 inches of water. The ESP modules were mounted inside the plate model and the measured pressures are referenced to the static pressure of the tunnel, as observed by a Pitot-static tube upstream of the splitter plate. The modules were automatically calibrated at regular intervals during a given test day. The pressure data was used to calculate the freestream velocity over the plate and to verify that the pressure gradient over the plate, in the area of interest, was zero. Flow visualization conducted in this tunnel suggests that the flow is two-dimensional in the zero pressure gradient region of the plate, with the exception of the region close to the side walls [3].

The synthetic jet utilized in this research effort featured a circular orifice 0.25 inches (6.35 mm) in diameter. The throat of the orifice is smoothly tapered from a diameter of 0.60 inches (15.2 mm) on the inside cavity wall to the 0.25 inch diameter exit dimension. The actuator design is shown schematically in Figure 2. The active element of the actuator was the wall of the cavity opposite the exit of the jet, the bottom wall in Figure 2. This wall was displaced electro-mechanically by a sinusoidal voltage. To document the in situ performance of the actuator, the displacement of the actuator diaphragm was recorded, as was the cavity pressure and temperature. Two dynamic pressure transducers were installed in the interior of the cavity, one transducer referenced to the static pressure of the tunnel upstream of the splitter plate and the other transducer is an absolute transducer. A thermocouple was also located in the cavity. The diaphragm displacement and cavity pressure as a function of phase can be seen in Figure 3. The presentation of all of the subsequent velocity measurements utilize this same phase reference. The diaphragm displacement is relative to the nominal cavity depth when the tunnel is on condition. This value is 1.68 mm.

Boundary Conditions

In addition to the boundary conditions associated with the actuator, i.e., the diaphragm displacement, cavity pressure and temperature, the boundary conditions for this case additionally consist of the upstream, or in-

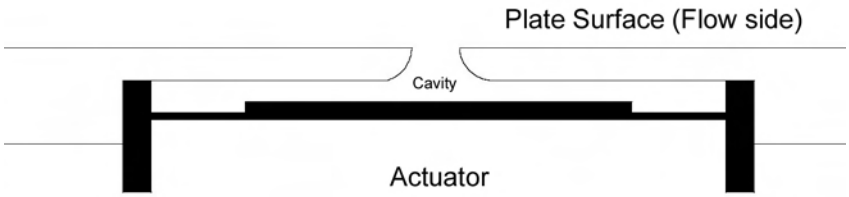

Figure 2: Schematic of the Synthetic Jet Actuator.

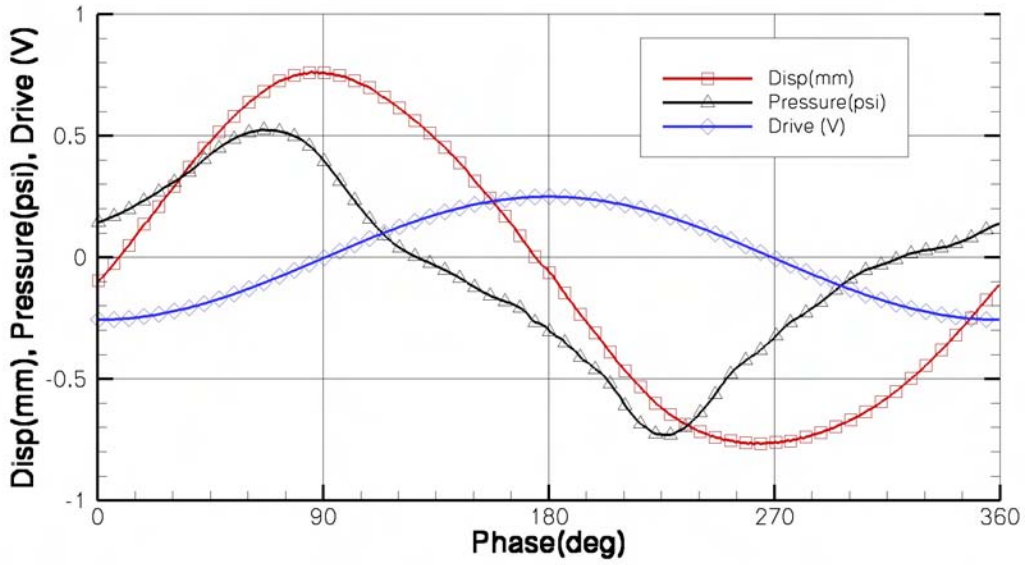

Figure 3: Diaphragm displacement, drive signal and cavity pressure as a function of phase for the Synthetic Jet Actuator.

flow, boundary condition, and the geometry of the model and the tunnel itself. The tunnel test condition was a Mach number in the test section over the plate of M = 0.10. The tunnel dimensions at the test section are 15.0 inches (381 mm) wide by 9.8 inch (249 mm) high (distance from the splitter plate to the top wall). The orifice diameter was 0.25±0.005 inches. The location of the jet orifice down the plate is specified in reference to the model coordinate system. The model coordinate system is shown schematically in Figure 4 and its origin was established where the first line of spanwise pressure taps intersects the line of centerline pressure taps. This location is 36.8 inches (935 mm) from the leading edge of the plate. In the model coordinate system, the centerline of the jet orifice is located at 2±0.020 inches (50.8±0.50 mm). Moving from the origin of the model coordinate system to the jet centerline in the streamwise direction defines the X coordinate axis, the Y coordinate axis is in the spanwise direction and the Z coordinate axis is in the vertical direction. The corresponding velocity components will be U, V, and W. From this point forward, distances in the streamwise, X, direction will be stated in millimeters or at times jet diameters from the jet centerline. The key locations are: x = 44.45 mm (-1D), x = 50.80 mm (0D, CL), x = 57.15 mm (1D), x = 63.50 mm (2D), x = 69.80 mm (3D), and x = 76.20 mm (4D).

While the atmospheric conditions varied on a daily basis, the conditions were never far from standard atmospheric conditions at sea level in a wind tunnel vented to the atmosphere, in a temperature-controlled room.

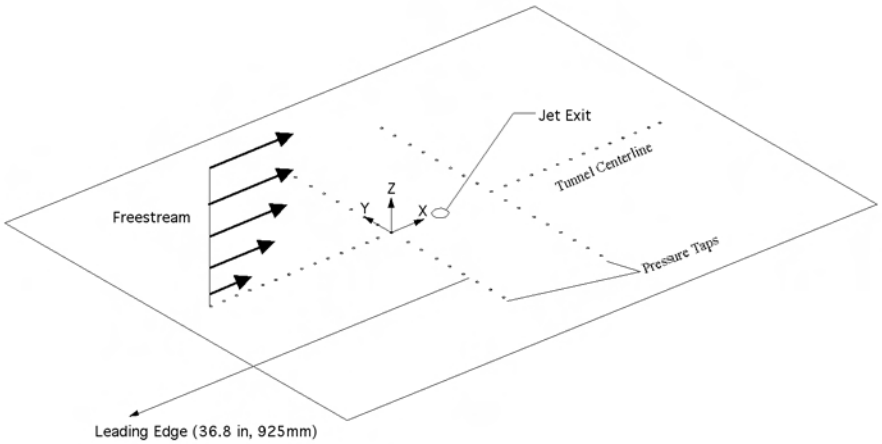

Figure 4: Schematic of the Model Coordinate System.

Freestream Mach Number	M_∞	0.10
Atmospheric Pressure	P_{atm}	101,325 Pa
Atmospheric Temperature	T_∞	23.9 °C (75 °F)
Density	ρ_∞	$1.185 kg/m^3$
Viscosity	μ_∞	$18.4x10^{-6} kg/ms$

Table 1: Atmospheric Conditions Observed for Case 2

These conditions are given in Table 1.

The upstream boundary conditions were measured at station x = 0.000 in the model coordinate system. A complete description of the state of the turbulent boundary layer was measured using the 3-component laser-Doppler velocimetry system to be described in the following section. All six components of the turbulent stress tensor were documented and presented as the upstream boundary condition. The velocity means and the turbulent stress components were compared to similar values available in the open literature, as shown for the mean profile of the freestream component of the velocity, U, in Figure 5.

Instrumentation and Data Acquisition

The velocity measurements to support Case 2 were carried out using a 3-component laser-Doppler velocimetry (LDV) system, a stereo (3D) digital particle image velocimetry (SDPIV) system, and a 2D digital particle image velocimetry (2D-PIV) system. The two PIV systems were the primary technique for measuring the velocity field. The LDV system was an orthogonal, crossed-fringe, fiber-optic probe configuration, with the probes mounted 90° from one another. The 514.5, 496.5, and 476.5 nanometer wavelengths from an Argon-Ion laser were used to measure the spanwise (V), vertical (W), and streamwise (U) velocity components, respectively within the tunnel. Bragg cells were utilized to provide directional measurement capability in all three velocity components. Both fiber optics probes used 750-mm focal length lenses, which along with an input beam diameter of 3 to 4mm, generated a sample volume calculated to be approximately 100 μm in diameter and spherical in shape. The optical setup of the LDV system can be seen in Figure 6. All velocity measurements were made in coincidence mode. Coincidence mode requires that a validated velocity signal be made independently in each of the three components within a very short time window, guaranteeing that

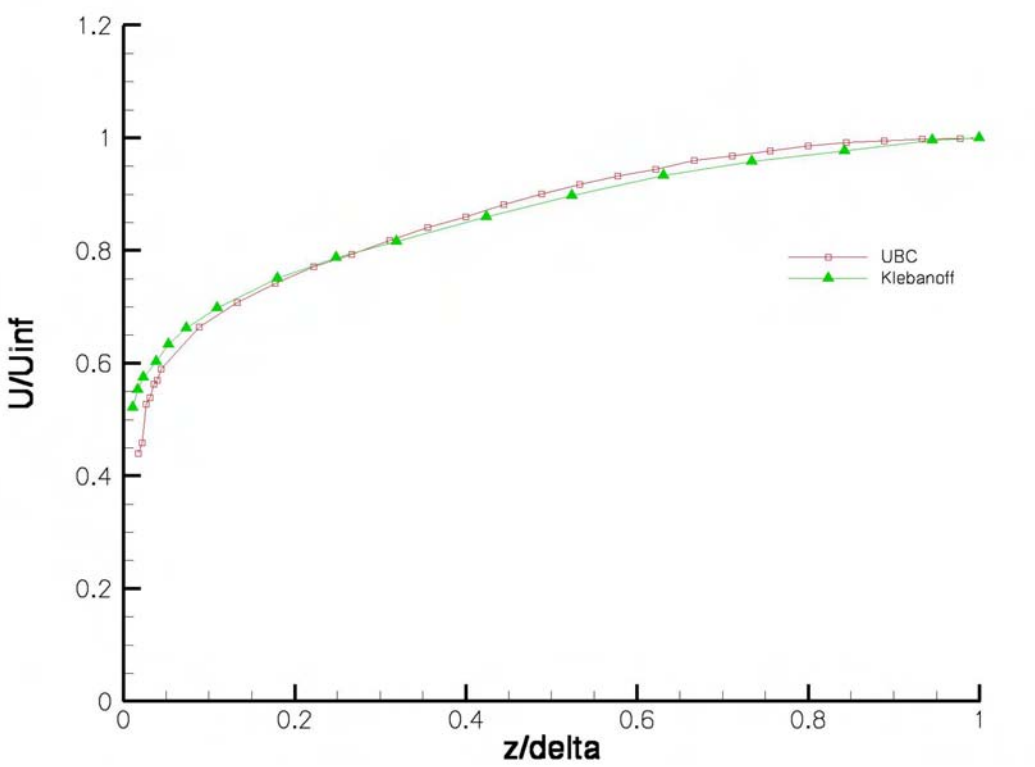

Figure 5: Upstream Boundary Condition on U compared to the data of Klebanoff[4]

the velocity signals come from a single particle traversing the measuring volume. The use of coincidence mode is required to make full turbulence measurements with an LDV system. The use of coincidence in the present research effort allows each of the six components of the turbulent stress tensor to be measured.

Additionally, the actuator drive and sync signal were acquired with each trigger and stored if the point was validated as being in coincidence. Consideration of the actuator drive and sync signal allows the LDV data, which is acquired at random intervals, to be reconstructed as a function of phase. The fiber optics probes were mounted on a X95 rail frame traversing system. The traversing system utilized several motorized slides that provided 1 meter of travel in each of the three axes, with 1 μm resolution in each direction. For the LDV portion of the experiment, the flow was seeded with mono-disperse, 0.86 μm polystyrene latex (PSL) micro-spheres. The seed particles were suspended in 100-proof alcohol and atomized by a six-jet atomizer. The atomized particles were then introduced into the settling chamber of the tunnel. The particles were fabricated at NASA Langley using the technique described by Nichols[2].

In processing the data from the LDV system, we wish to relate the velocities measured to a particular phase of the actuator. The LDV system acquires, along with the coincident velocity data, data for the drive signal of the actuator and a sync signal. Analysis of these values allows for the reconstruction of the phase angle at the time of acquisition and was used to phase average the LDV data record at every point. Once the phase angle of each piece of LDV data is calculated, the data can be grouped into bins according to phase angle. Each bin represents data with a phase angle in a certain range. For the data in Case 2, this range was 10°. The bin was then averaged to yield the phase-average at that point. The uncertainty in the phase-averaged LDV mean data is estimated to be $\pm$0.5%. Once all the phase-averaging was accomplished, each of the phase-averaged series was averaged as a time series to calculate the long-time average at each point. The long-time average velocity profiles derived from the LDV data are shown in Figure 7.

The timing control, image acquisition, data management and post-processing of both the stereo PIV and the 2-D PIV data was handled by a commercial system. The light source utilized was a pulsed, frequency-

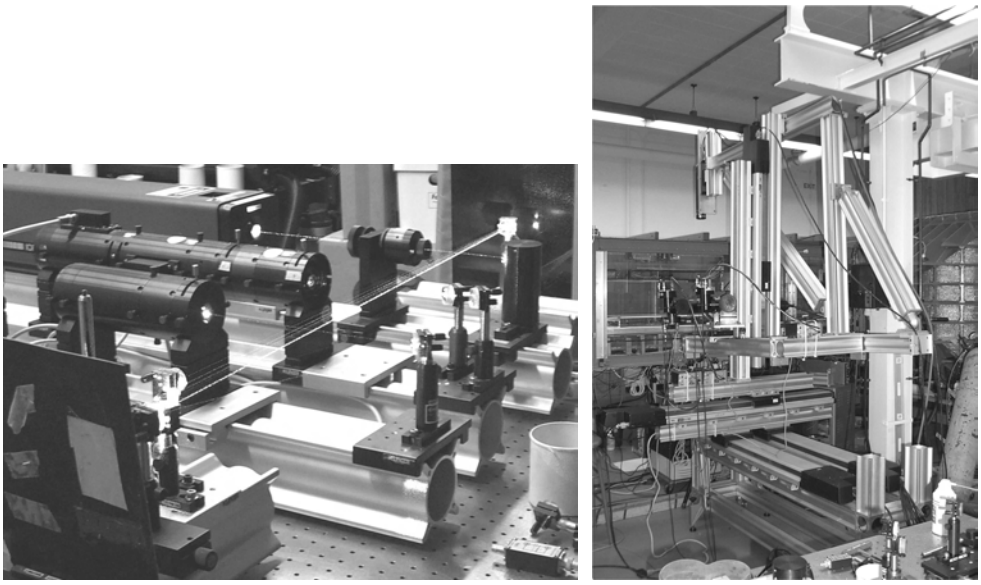

(a) Laser and Optical Configuration

(b) Fiber Optic Bundles and Traversing System

Figure 6: The Laser-Doppler Velocimetry Setup.

doubled 300 mJ Nd-YAG laser operating at 10 Hz. For the PIV portion of the experiment, the flow within the tunnel was seeded with atomized mineral oil with a typical particle size of 2 microns. The seed was injected into the flow in the tunnel settling chamber. Standard sheet-forming optics were utilized and the cameras were positioned on opposite sides of the tunnel for the SDPIV data. Also for the SDPIV, the camera mounts allow for the required tilting of the lens, relative to the camera body, in order to satisfy the Scheimpflug condition. The light sheet orientation for the SDPIV data was in the spanwise direction and in the streamwise direction for the 2D-PIV data. The position of the sheet in the spanwise direction was controlled by a prism mounted on the same traversing system utilized by the LDV system. The light sheet thickness was typically 1.5 mm thick. The resolution of each camera was 1008 x 1018 pixels and the typical field of view was 40 mm x 40 mm for the SDPIV and 18 mm x 18 mm for the 2D-PIV.

The image acquisition and lasers for both PIV systems were synchronized with the drive signal of the actuator so that images could be acquired at a specific time delay after the beginning of a cycle of the actuator drive signal. A specific delay for the laser pulsing and image acquisition corresponds to a specific phase of the actuator drive cycle. The same sync signal that the LDV system acquired was used as the trigger for the PIV signal. Within the PIV software, the timing delay was varied in order to acquire data at 36 specific phases of the synthetic jet actuator drive signal, equally spaced over both the exhaust and suction cycles. The flowfield over the entire drive signal was recorded as 10,800 instantaneous velocity fields, 300 velocity field measurements at each of 36 specific delays, which results in the measurement of the velocity field every 10 degrees of phase. The 300 image pairs were acquired over a period of 3 minutes and were processed using a standard PIV cross-correlation data reduction technique and then averaged to give the phase-averaged, or ensemble-averaged, velocity field. The uncertainty in the phase-averaged 2D-PIV mean data is estimated to be $\pm$1.3%. These phase-averaged velocity fields were be ordered in time allowing the evolution of the jet-induced velocity field, and its interaction with the crossflow, to be studied. The long-time average of the velocity field was calculated by averaging, through one complete cycle, the individual phase-averaged velocity fields, as shown in Figure 8 for data derived from the 2-D PIV system.

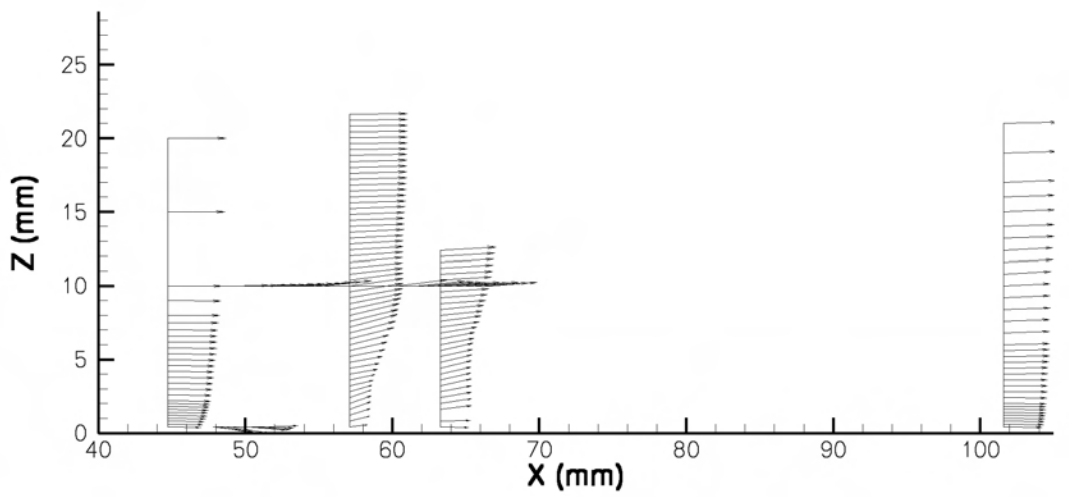

Figure 7: Long-Time Average Velocity Profiles from the LDV data.

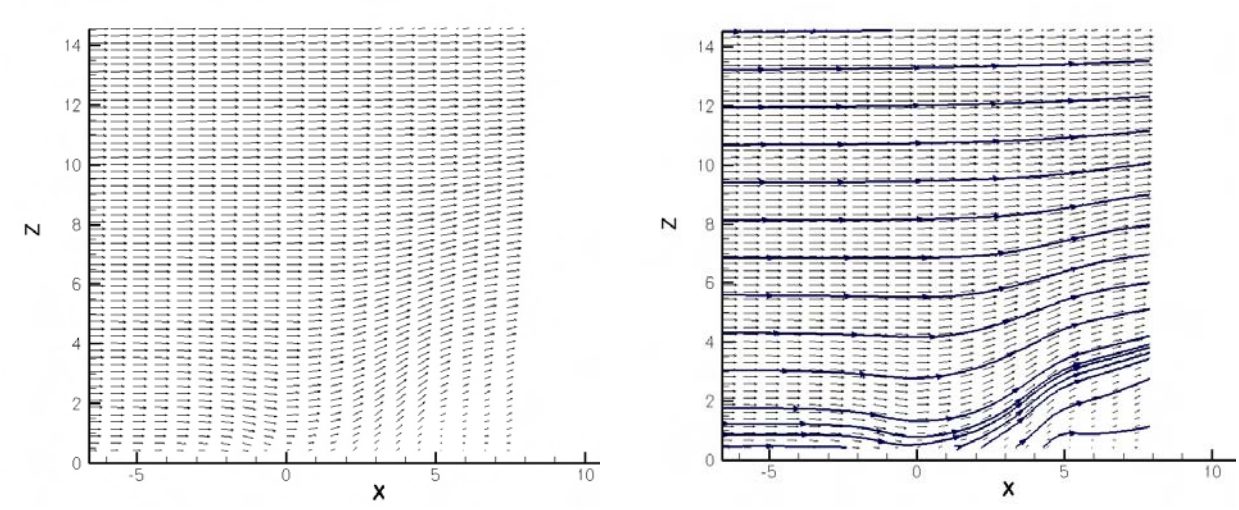

(a) Velocity Vectors

(b) Velocity Vectors and Streamlines

Figure 8: Long-time average Velocity Field via 2-D PIV. In these figures, x = 0 corresponds to X = 50.325 mm in the model coordinate system.

References

[1] Schaeffler, N. W. “The Interaction of a Synthetic Jet and a Turbulent Boundary Layer,” AIAA Paper No. 2003-0643, 2003.

[2] Nichols, C. E., “Preparation of Polystrene Microspheres for Laser Velocimetry in Wind Tunnels,” NASA TM-89163, 1987.

[3] Jenkins, L., Althoff Gorton, S., and Anders, A., “Flow Control Device Evaluation for an Internal Flow with an Adverse Pressure Gradient,” AIAA Paper No. 2002-0266, 2002.

[4] Klebanoff, P. S., “Characteristics of Turbulence in a Boundary Layer with Zero Pressure Gradient,” NACA TR-1247, 1953.